



# Was the strengthening of the Northern polar vortex in 2024/2025 associated with the Hunga Tonga eruption?

Ales Kuchar<sup>1</sup>, Matthias Stocker<sup>2</sup>, Alistair Bell<sup>3</sup>, Bruno Lehner<sup>1</sup>, Jessica Kult-Herdin<sup>1</sup>, Gabriel Chiodo<sup>4</sup>, Timofei Sukhodolov<sup>5</sup>, Eugene Rozanov<sup>5,6</sup>, Gunter Stober<sup>3</sup>, and Harald E. Rieder<sup>1</sup>

<sup>1</sup>Institute of Meteorology and Climatology, BOKU University, Vienna, Austria

<sup>2</sup>Wegener Center for Climate and Global Change, University of Graz, Graz, Austria

<sup>3</sup>Institute of Applied Physics, Microwave Physics, University of Bern, Switzerland

<sup>4</sup>Instituto de Geociencias (IGEO), CSIC-UCM, Madrid, Spain

<sup>5</sup>Physikalisch-Meteorologisches Observatorium Davos/World Radiation Center (PMOD/WRC), Davos, Switzerland

<sup>6</sup>Ozone Layer and Upper Atmosphere Research Laboratory, Saint Petersburg State University, Russian Federation

**Correspondence:** A. Kuchar (ales.kuchar@boku.ac.at)

**Abstract.** The 2022 Hunga Tonga (HT) eruption injected an unprecedented amount of water vapour (WV) into the stratosphere and mesosphere, emerging as a potential multi-year driver of variability in those layers and associated climate feedbacks. Using satellite and reanalysis datasets, and ensemble simulations with the SOCOLv4 model, with and without the HT forcing, we diagnose the chain of processes linking the eruption to the exceptionally strong Northern Hemisphere stratospheric polar vortex (SPV) observed in winter 2024/2025. Satellite data show "tongues" of enhanced WV (up to 2 ppmv above climatology) descending from the mesosphere into the polar stratosphere, collocated with ozone reductions and persistent cold anomalies of about 5–15 K, alongside a record-strong SPV. Our model can reproduce the main structure of the descending plume, its effects on chemistry, and the SPV strengthening, albeit with underestimated magnitudes and an earlier onset than observed. Offline radiative transfer calculations indicate that the WV and ozone anomalies drive net radiative cooling over the polar stratosphere, sharpening meridional temperature gradients and thereby intensifying the vortex. The observed 2024/2025 winter thus represents a plausible manifestation of HT-induced vortex variability, with simulations also indicating a shift toward sudden stratospheric warmings in the winter 2025/2026 as the WV forcing declines.

## 1 Introduction

The 2022 Hunga Tonga (HT) eruption was unprecedented in terms of i) injection altitude up to 57 km (Proud et al., 2022), ii) the observational coverage of a direct water vapor (WV) injection of this magnitude (Vömel et al., 2022), and iii) the radiatively-driven plume descent shortly after the eruption due to the highly localized moist volcanic cloud (Kroll and Schmidt, 2024). Many studies have been dedicated to the impacts of the HT eruption, including changes in stratospheric and mesospheric composition (Evan et al., 2023), radiation (Stocker et al., 2024; Randel et al., 2024b), and direct (Jenkins et al., 2023; Schoeberl et al., 2023; Stenchikov et al., 2025) and indirect (Bednarz et al., 2026; Kuchar et al., 2025) climate impacts.

The WV inputs of HT were distributed throughout the stratosphere, even to the mesosphere. Randel et al. (2024a) documented positive residuals of WV over high latitudes in both hemispheres, tied to the downward transport of WV from the HT



eruption. Modelling (Fleming et al., 2024; Zhou et al., 2024; Kuchar et al., 2025; Zhuo et al., 2025) and observational (Millán et al., 2022; Schoeberl et al., 2025) studies suggest that the anomalous WV induced by the HT eruption in 2022 should diminish within 5–7 years, and that Antarctic dehydration will remain the dominant WV removal pathway (Zhou et al., 2024). Therefore, we expect that the Brewer-Dobson circulation is responsible for the downward transport of WV over middle and high latitudes during the wintertime, in analogy to the downward transport of NO<sub>x</sub>, produced by energetic particle precipitation, inside the polar vortex (e.g. Funke et al., 2014).

Kuchar et al. (2025) explored a novel pathway by which water-rich volcanic eruptions, such as HT may modulate stratospheric and mesospheric conditions and influence regional surface climate. Their targeted model simulations illustrated that the excess WV can reduce meridional temperature gradients near the stratopause, leading to a negative Northern Annular Mode anomaly that propagates to the surface in late winter. Several features were reproduced by an independent atmosphere-only simulation using the NCAR model (Bednarz et al., 2026, and accompanying discussion), including mesospheric cooling at lower latitudes, which, via the thermal wind relation, has the potential to weaken the polar-night jet. Taken together, these studies suggest that HT may have provided favorable conditions for Sudden Stratospheric Warmings (SSWs) observed in NH winters following the HT eruption.

Various atmospheric (and surface) signals have also been linked to the stratospheric WV increase. Joshi et al. (2006) showed a strengthening of the stratospheric jet in boreal winter associated with the cooler lower stratospheric midlatitudes (increase of meridional temperature gradient) in response to an increased stratospheric WV. Maycock et al. (2013) and Seabrook et al. (2023) reported similar circulation response. This feature was indeed observed in the winter 2024/2025 when the stratospheric polar vortex was anomalously strong, reaching the climatological maximum ( $\sim 61.19 \text{ ms}^{-1}$ ) on December 24, 2024 (see Fig. 1A). There were only a few recent winters with a similarly strong and stable polar vortex in the Northern Hemisphere, i.e. 2010/2011, 2015/2016, and 2019/2020 (Manney et al., 2011; Matthias et al., 2016; Lawrence et al., 2020; Andrews and McIntyre, 1987; Rieder et al., 2025).

Motivated by the diverse findings of HT impacts summarized in the recent dedicated report (APARC, 2025), our study seeks to extend the portfolio of pathways by which the HT eruption may have modulated stratospheric and mesospheric conditions and consequently impacted the surface climate. Specifically, we aim here to answer the following questions: i) How does the long-term response of the stratospheric polar vortex (SPV) to atmospheric composition changes following the HT eruption differ from the short-term response? ii) Did atmospheric composition changes precondition SPV states, particularly the strong SPV observed in 2024/2025? and iii) if so, which predictive power can be derived from comprehensive chemistry-climate model simulations for SPV states in the coming years?

To this end, we provide a combined observational and modelling assessment of the 2024/2025 event and its linkages to the lingering Hunga-induced moist plume. We use a reanalysis and observations from MLS and SWOOSH (Appendix A1), together with large-ensemble SOCOLv4 simulations with and without the HT forcing (Appendix A2), to investigate the sensitivity of the circulation to excess WV from HT and assess the chain of processes leading to SPV strengthening.

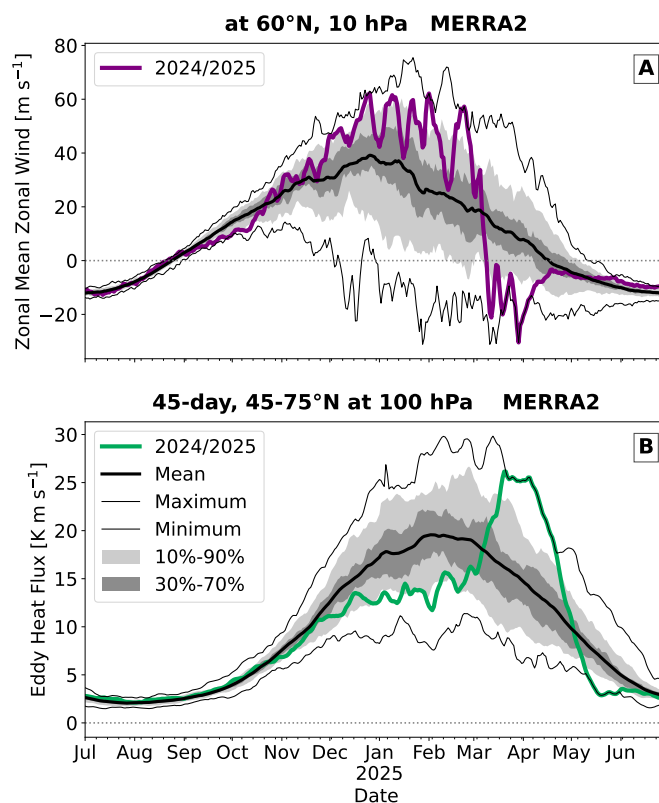


**Figure 1. A:** The average (east-west) zonal wind for 60°N at 10 hPa for the extended winter 2024/2025 (OW3) in MERRA2. This is near the peak of the polar jet maximum. **B:** The eddy heat flux averaged between 45°N and 75°N at 100 hPa for the 45 days before the date indicated.

## 55 2 Results

### 2.1 Observed changes in water vapor, ozone, and temperature

We set the scene by illustrating the daily evolution of stratospheric dynamics in the extended winter 2024/2025 (the third observed winter after the HT eruption; thus, marked as OW3) using the MERRA2 reanalysis in Fig. 1. Here, the zonal-mean winds diagnosed at 60°N at 10 hPa illustrate the enormous strength of the SPV. Next, we turn the focus to anomalies of WV, temperature, and ozone (derived from the MLS observations in Fig. 2), to put the exceptionally strong SPV in the context of the lingering HT perturbation in polar latitudes. The WV anomalies (see Fig. 2A) are characterized by “tongues” with concentrations of up to 2 ppmv. The first “tongue” appears in the mesosphere during October/November 2024 and continuously propagates downward with time to ~10 hPa, where it gradually weakens and dissipates by March 2025, when it merges with the stratospheric background. A second “tongue” forms in the mesosphere in January 2025 and also propagates downward.

65 The WV anomalies are partly collocated with negative ozone (< 0.5 ppmv) and temperature anomalies in the stratosphere and lower mesosphere (see Fig. 2B, C). These anomalies are followed by their positive counterparts, which also descend



downward with time. By October, an enhanced ozone anomaly ( $\sim 0.5$  ppmv) emerged around 10 hPa, leading to effective warming due to ozone absorption of solar radiation and thereby masking the WV-induced cooling propagating downward. In March, we observe a significant increase in both temperature and ozone, which corresponds to the stratospheric final warming during which the SPV does not recover and transitions to summer conditions, with easterly winds across the stratosphere (see Fig. 1A). The by then observed stratospheric and lower-mesospheric longwave cooling rates are dominated by CO<sub>2</sub> together with ozone and WV (Clough and Iacono, 1995; Brasseur and Solomon, 2005). The close correspondence between the WV and ozone anomalies and the diagnosed temperature response suggests that they are the primary drivers of the initial cooling observed in OW3. We examine this mechanism explicitly in the model simulations below.

## 75 2.2 Modeled changes in water vapor, ozone, and temperature

The downward propagating "tongue" of WV during winter is captured in our SOCOLv4 ensemble. The feature emerges in the extended winter 2023/2024 (marked as second model winter after the HT eruption, MW2; see Fig. 3A) and winter of 2024/2025 (MW3; see Fig. 4A). The WV enhancement is, however, underestimated compared to observations in Fig. 2A, especially in MW3. Given the well documented model deficiency of accelerated transport of SOCOLv4 (discussed in detail in Appendix A2), we argue that the winter MW2 in our simulations corresponds to OW3 in observations (see Section 2.1 and Fig. 2). For the MW2 SOCOLv4 yields a similar strengthening of the vortex with not as pronounced weakening as observed at the end of OW3 (cf. Fig. 3D and Fig. 1A). In analogy, we understand MW3 as the upcoming OW4, as we detail further below.

For MW2 (equaling OW3) we attribute the initial ozone destruction in the upper stratosphere and lower mesosphere to increased OH concentrations induced by the excess WV from the HT eruption (HO<sub>x</sub> cycle) and the ClO<sub>x</sub> activation from chlorine reservoirs (see Fig. A2). These coincide with a negative anomaly in NO<sub>x</sub> mainly attributable to cooling at these levels (Fleming et al., 2024). In contrast, as reported in Fleming et al. (2024); Kuchar et al. (2025), the positive ozone anomaly in the middle stratosphere emerges due to increased conversion of NO<sub>x</sub> to the HNO<sub>3</sub> reservoir given overall higher abundance of OH. Further negative ozone and negative temperature anomalies are associated with stronger SPV and correspondingly weaker poleward transport of ozone from lower latitudes.

Next, we investigate the radiative effect of the observed changes in WV and O<sub>3</sub> on temperature via offline radiative transfer (RT) calculations (see Appendix A3). These RT calculations reveal that perturbations in both WV and ozone abundances are capable of inducing temperature anomalies in the order of  $-5$  to  $-15$  K, with ozone dominating the change in heating rates in the upper layers. These temperature anomalies are comparable with those observed (see Fig. 2C) and simulated (see Fig. 3C). SOCOLv4, however, does yield a more muted temperature response initially, attributable to more muted changes in shortwave heating rates following the weaker ozone anomaly than seen in the MLS observations.

The negative temperature anomalies throughout the upper stratosphere and lower mesosphere result in an enhanced meridional temperature gradient, which strengthens, via the thermal wind balance, SPV. The SPV strengthening may initially enhance vertical wave propagation during October, a time when zonal winds (ZW) are usually weak and thus allow more planetary waves (PWs) to propagate upwards into the stratosphere (Charney and Drazin, 1961). In this respect, we understand the simultaneously observed anomalously high eddy heat flux (EHF) at 100 hPa (see Fig. 1B) as a proxy for upward propagation of

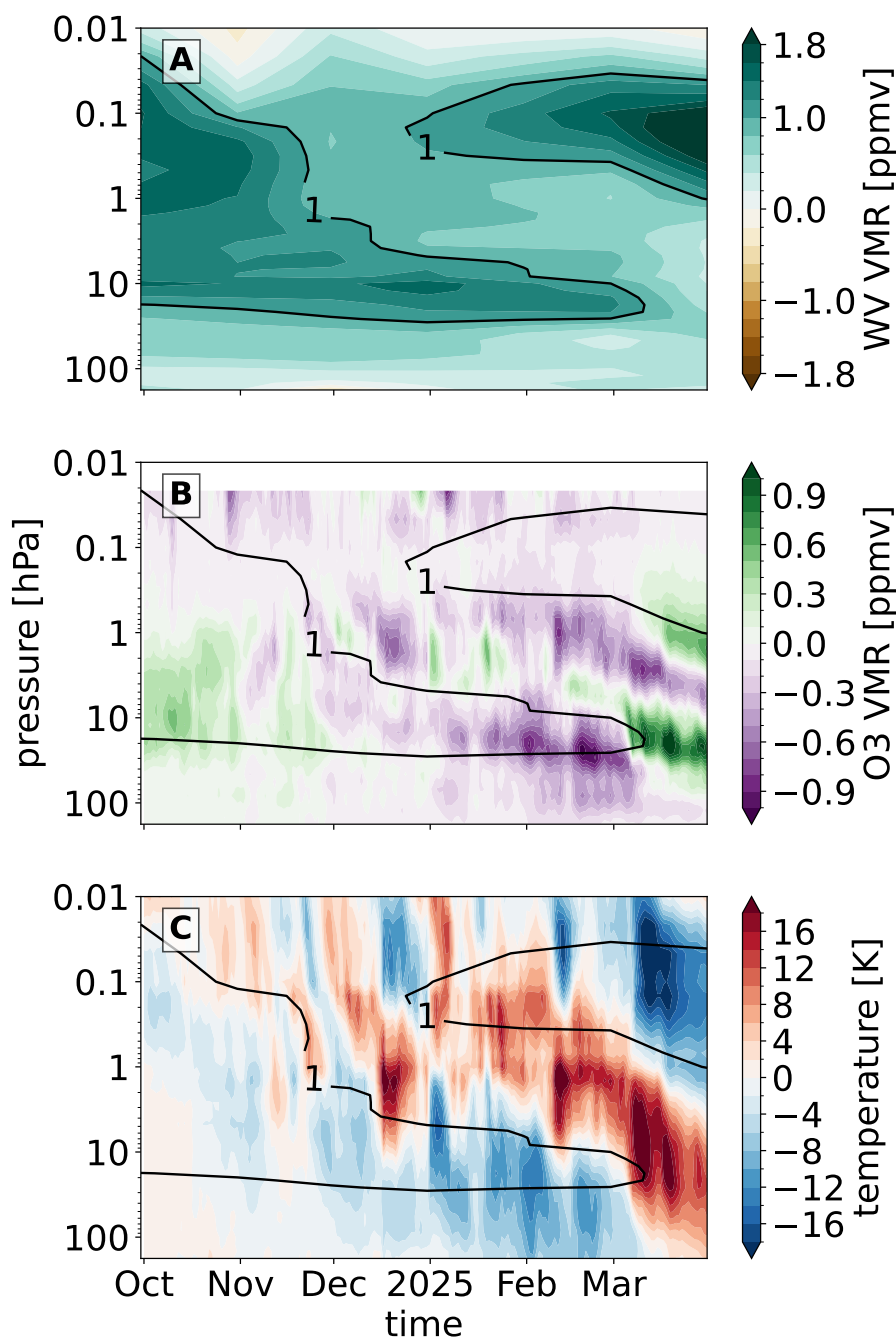


**Figure 2.** Zonal mean weighted average for latitudes between  $60^{\circ}$ – $90^{\circ}$ N of water vapour volume mixing ratio (VMR; shading in A and contour of 1 ppmv in B and C; in ppmv; monthly), ozone VMR (shading in B, in ppmv; daily) and temperature (shading in C; in K; daily) and anomalies for the extended winter 2024/2025 (OW3) from MLS. Anomalies are expressed as differences with respect to the climatology for the period 2006–2020. Due to missing data, water vapour is visualized as monthly anomalies with interpolated gaps. Due to a retrieval artifact in the 10–8 hPa layer we smoothed the data vertically (see Appendix A1).



PWs (e.g. Newman et al., 2001). This way we associate the anomalously weak ZW below in the stratosphere due to anomalously breaking PWs (Appendix A5). As the cooling progresses downward, it aids the strengthening of the winds, which tend to be too strong for wave propagation (Plumb, 1989). This may confirm the nonlinearity of SPV for generally large wave forcing during the NH winter conditions (Scott and Haynes, 2002). The stronger SPV is associated with pronounced negative and positive temperature anomalies below and above, respectively. A similar dipole structure has been discussed in studies diagnosing SH high-latitude temperature trends as a consequence of ozone depletion (e.g Young et al., 2013; Keeble et al., 2014). Manzini et al. (2003) attributed the positive temperature anomaly at upper levels to increased downwelling, and thus, consequently, adiabatic warming due to enhanced gravity wave propagation. Correspondingly, stronger westerlies in the stratosphere filter eastward gravity waves while westward gravity waves propagate freely upward and deposit their momentum above.

As for MW2, we find similar "tongues" of WV and downward propagation of ozone in the SOCOLv4 simulations for MW3 (see Fig. 4). Here, however, the excess of WV only yields up to 0.25 ppmv, and thus a much smaller magnitude compared to MW2 and OW3 by MLS. This reduced WV forcing results only in a subtle cooling, which slightly strengthens the ZW, before they significantly weaken as a consequence of anomalously high EHF in December 2024 and the beginning of January 2025. This episode is followed by a recovery of SPV and collocated negative temperature anomaly propagating from the lower mesosphere to the lower stratosphere (discussed in detail in Appendix A7). In Appendix A7 we also argue that the winter 2025/2026 (OW4) bears an enhanced probability for SSW occurrence.

### 3 Discussion and summary

Our study addresses the question of whether the anomalously strong Northern Hemisphere stratospheric polar vortex (SPV) of the boreal winter 2024/2025 has been linked to lingering dynamical and radiative impacts of the HT eruption. For this time period, satellite data show a coherent descent of HT-related water-vapour anomalies into the high-latitude stratosphere, collocated with a marked reduction in ozone and pronounced cold anomalies in the upper stratosphere and lower mesosphere. We detail that an ensemble of SOCOLv4 simulations, with the HT forcing, is able to reproduce the main spatial patterns of this WV plume and associated ozone response. Furthermore, through offline radiative transfer calculations, we show that the WV and ozone anomalies are, in combination, sufficient to generate substantial radiative cooling, which sharpens the meridional temperature gradient and strengthens polar stratospheric westerly winds.

The proposed mechanism, in which excess WV from HT and associated ozone changes drives radiative cooling that preconditions the polar vortex, is partly analogous to the well-documented Southern Hemisphere response to Antarctic ozone depletion in the lower stratosphere and EPP-driven effects from mesospheric levels downward (Seppälä et al., 2025). Here, however, excess stratospheric WV from HT is considered as the primary driver. The key elements are the slow Brewer–Dobson descent of the HT WV anomaly, enhanced HO<sub>x</sub> and ClO<sub>x</sub> chemistry leading to upper-stratospheric/mesospheric ozone loss, and the resulting longwave and shortwave cooling where WV and ozone anomalies overlap. This cooling steepens the high-latitude temperature gradient and, via the thermal-wind balance, intensifies the vortex, thereby inhibiting further upward propagation of planetary waves and favouring a strong-vortex regime. At the same time, the response is strongly nonlinear: early-autumn

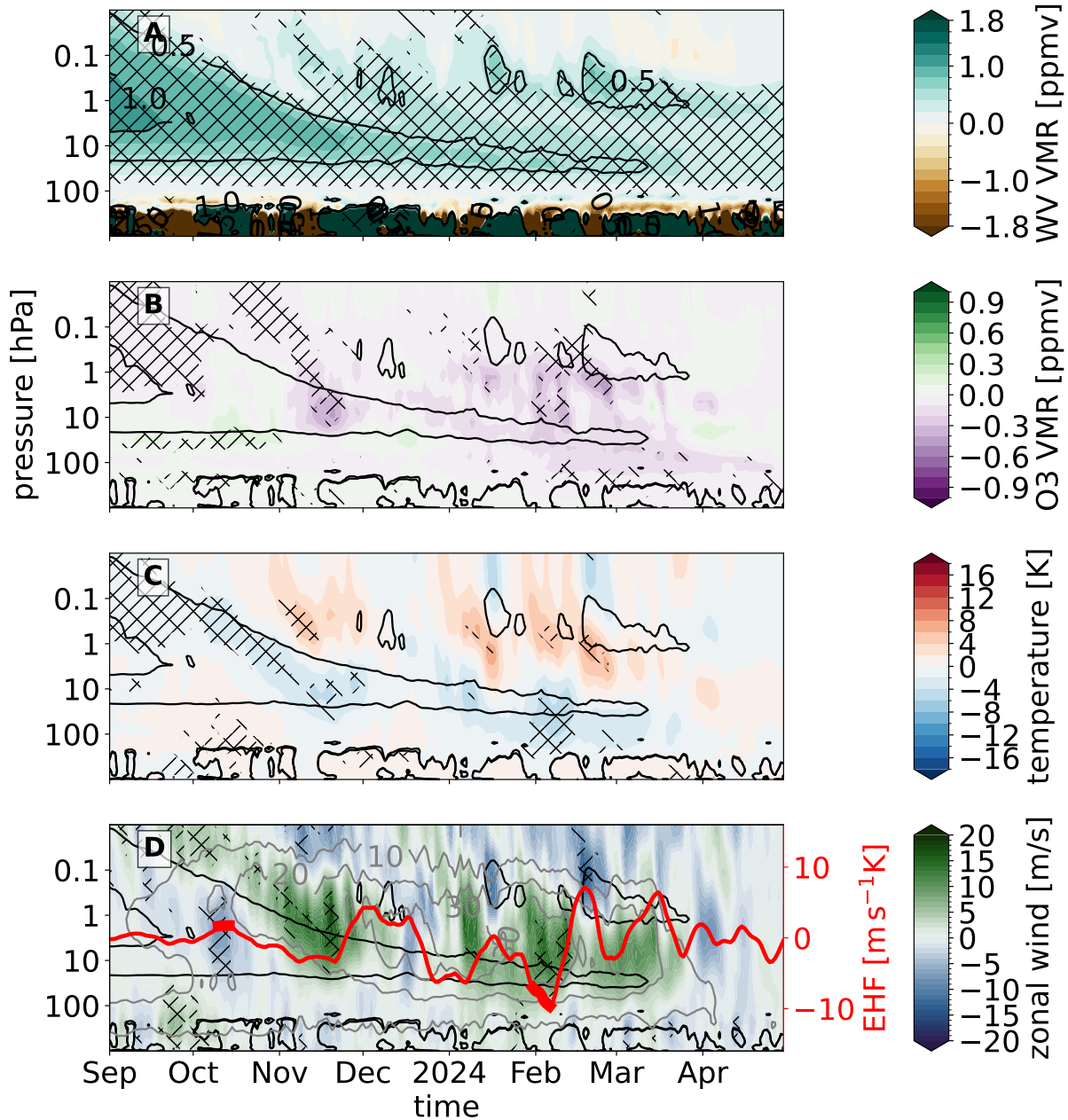


**Figure 3.** Weighted zonally-average over  $60^{\circ}$ – $90^{\circ}$ N of water vapour volume mixing ratio (VMR; shading in **A** and contours of 0.5 and 1 ppmv in **A**, **B**, **C** and **D**; in ppmv), ozone VMR (shading in **B**, in ppmv), temperature (shading in **C**; in K), and zonal wind at  $60^{\circ}$ N (shading in **D**) and Eddy Heat Flux at 100 hPa averaged over  $45^{\circ}$ – $75^{\circ}$ N (EHF in  $\text{m s}^{-1}\text{K}$ ; red line in **C**) daily anomalies for the extended winter 2023/2024 (MW2) from SOCOLv4. Anomalies are expressed as the difference between the SOCOLv4 simulation with and without the HT forcing. Hatching  $\backslash\backslash\backslash$  and  $\backslash\backslash\backslash\backslash$  shows where the p-values of the t-test are  $< 0.1$  and  $< 0.05$ , respectively. Gray contours in **D** represent absolute values of zonal wind in the SOCOLv4 simulation with the HT forcing.

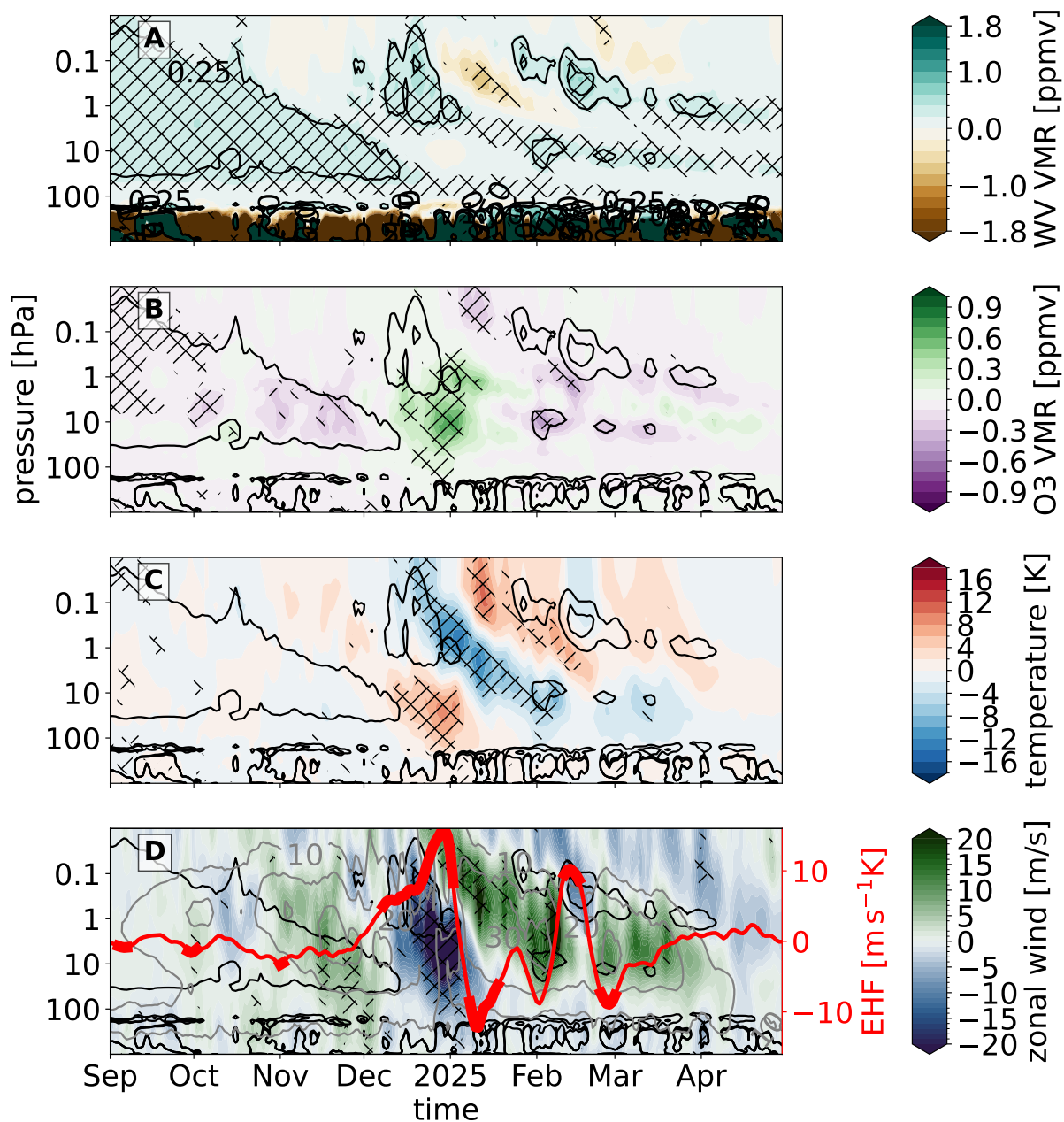


Figure 4. As in Fig. 3 but for the extended winter 2024/2025 (MW3).



135 wave activity can still transiently weaken the vortex, but once the radiatively strengthened westerlies have reached critical strength, additional wave forcing shows limited impact. The observed 2024/2025 winter (OW3) thus appears as a plausible manifestation of HT-induced vortex variability, rather than a uniquely forced event.

140 Several limitations temper the interpretation and generality of these findings. One reason is that the too fast transport in SOCOLv4 causes the model to simulate the analogous 2024/2025 winter approximately one year earlier. SOCOLv4 also underestimates the amplitude of the HT-induced WV anomaly when compared with satellite records, implying that our simulated radiative cooling and dynamical response are likely conservative. However, SOCOLv4 agrees well with other models (Zhuo et al., 2025) in terms of the water vapor e-folding time (cf. Kuchar et al., 2025, Section A1). The radiative cooling and heating estimates rely on idealized offline calculations and thus cannot fully capture the coupling between radiation, atmospheric composition, and dynamics. Our analysis is also based on a single model with a specific configuration (Sukhodolov et al., 2021, and references therein). In addition, internal variability associated with ENSO and other tropospheric sources of internal variability may be only partially sampled by 10 ensemble members (e.g. Bittner et al., 2016a; Bednarz et al., 2026). On the other hand, a sufficiently strong (volcanic) forcing can produce a robust, stronger-than-average NH polar vortex (Bittner et al., 2016b).

150 Despite these caveats, our findings support the view that HT-induced WV and ozone anomalies have become an important multi-year driver of high-latitude winter variability. In fact, our current study and previous research detail a clear dichotomy: manifesting on the early-time scale as SPV weakening (Kuchar et al., 2025) and on the long-time scale as SPV strengthening. Furthermore, looking ahead, our ensemble simulations suggest that as the WV plume continues to descend and QBO/ENSO conditions evolve, the balance between strong-vortex winters and SSW-prone winters may shift once more in 2025/2026 because of the upcoming weaker WV forcing (see recent observed WV (less than 1 ppmv), ozone and temperature anomalies in Fig. A3), with corresponding impacts on surface patterns. More generally, unprecedented eruptions like HT may act as intermittent “sources of predictability” also called “windows of forecast opportunity” for polar winter circulation (Rupp et al., 2025, and references therein), albeit in a fundamentally probabilistic sense.

160 *Code and data availability.* SWOOSHv2.7 data can be downloaded from <https://csl.noaa.gov/groups/csl8/swoosh/>. The MERRA2 reanalysis dataset postprocessed by the NASA Ozone Watch can be downloaded for zonal wind and eddy heat flux from [https://ozonewatch.gsfc.nasa.gov/meteorology/figures/merra2/wind/u60n\\_10\\_2024\\_merra2.txt](https://ozonewatch.gsfc.nasa.gov/meteorology/figures/merra2/wind/u60n_10_2024_merra2.txt) and [https://ozonewatch.gsfc.nasa.gov/meteorology/figures/merra2/heat\\_flux/vt45\\_75-45n\\_100\\_2024\\_merra2.txt](https://ozonewatch.gsfc.nasa.gov/meteorology/figures/merra2/heat_flux/vt45_75-45n_100_2024_merra2.txt), respectively. Any direct access to full simulation data can be arranged by contacting the authors. The code and data that was used to produce all plots in this study will be made available upon the publication.

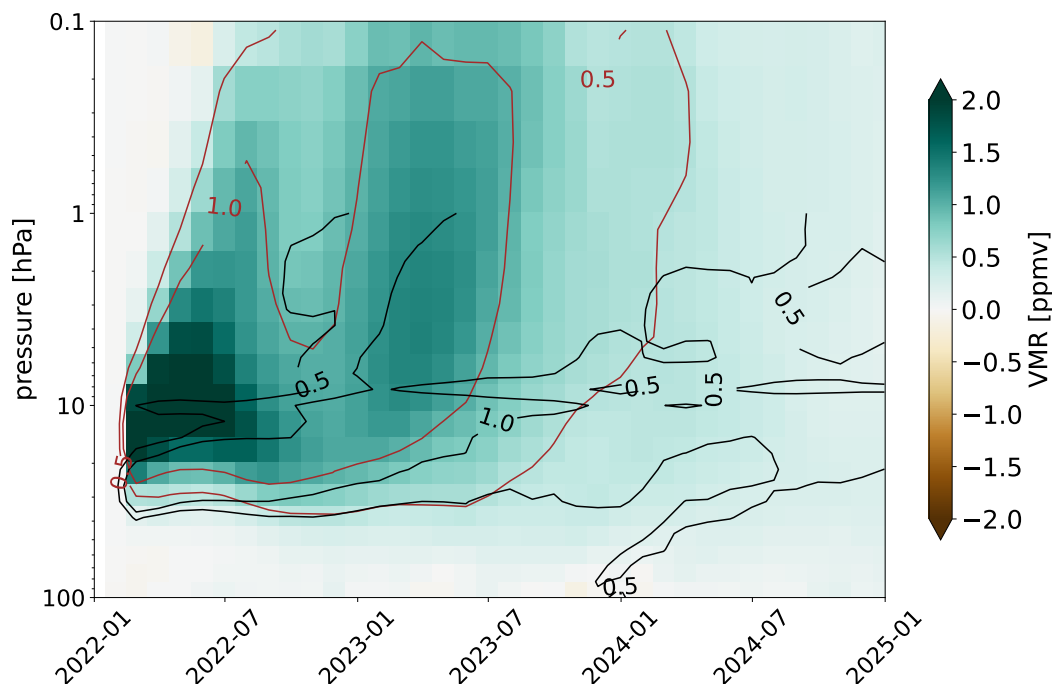


**Figure A1.** Globally averaged WV anomaly in SOCOLv4 (shading and brown contours for 0.5 and 1 ppmv) and SWOOSH (black contours for 0.5 and 1 ppmv) for the period 202201–202501.

## Appendix A: Methods

### A1 Observational datasets

#### A1.1 MERRA2

We visualized meteorological variables (zonal wind and eddy heat flux) from the MERRA2 reanalysis (Gelaro et al., 2017) 165 postprocessed by the NASA Ozone Watch (Kramarova and Lait, 2025) for the winter 2024/2025 (see Fig. 1).

#### A1.2 MLS

The Microwave Limb Sounder (MLS; Waters et al., 2006) instrument onboard NASA's Aura satellite has been operational since 2004 and provides near global (82°S—82°N) measurements of key atmospheric constituents and temperature based on thermal microwave emissions along the Earth's limb. The MLS provides about 3500 vertical profiles per day for each species. 170 The profiles have a vertical resolution of approximately 3 to 5 km in the stratosphere and 6 to 8 km in the mesosphere. In this study, we use Version 5 of the retrieval products for water vapor, ozone, and temperature (Livesey et al., 2022).

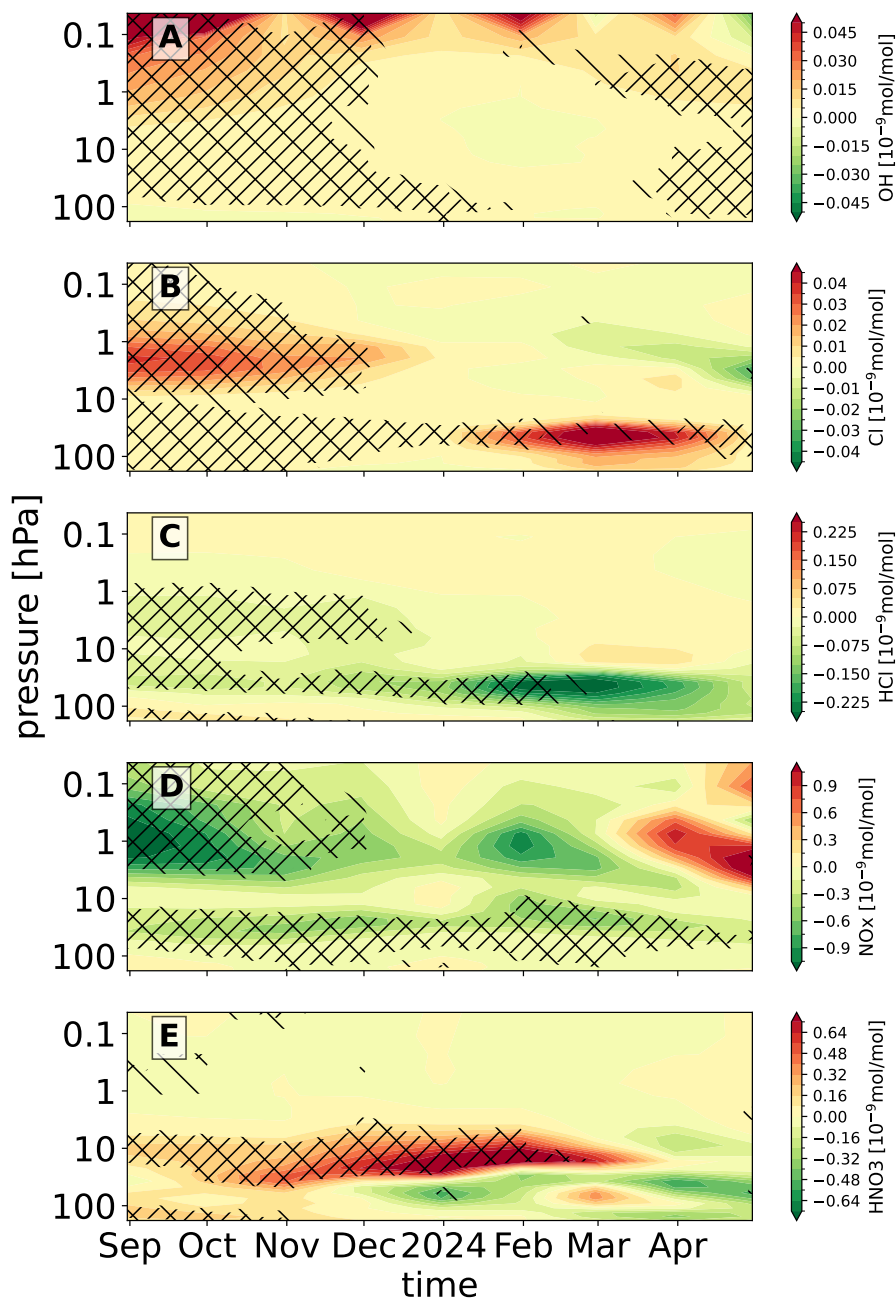


**Figure A2.** Monthly zonal-mean anomalies of polar chemistry for the period 2023/2024. Anomalies are expressed as the difference between the SOCOLv4 simulation with and without the HT forcing. Hatching  $\backslash\backslash\backslash$  and  $///$  shows where the p-values of the t-test are  $< 0.1$  and  $< 0.05$ , respectively.

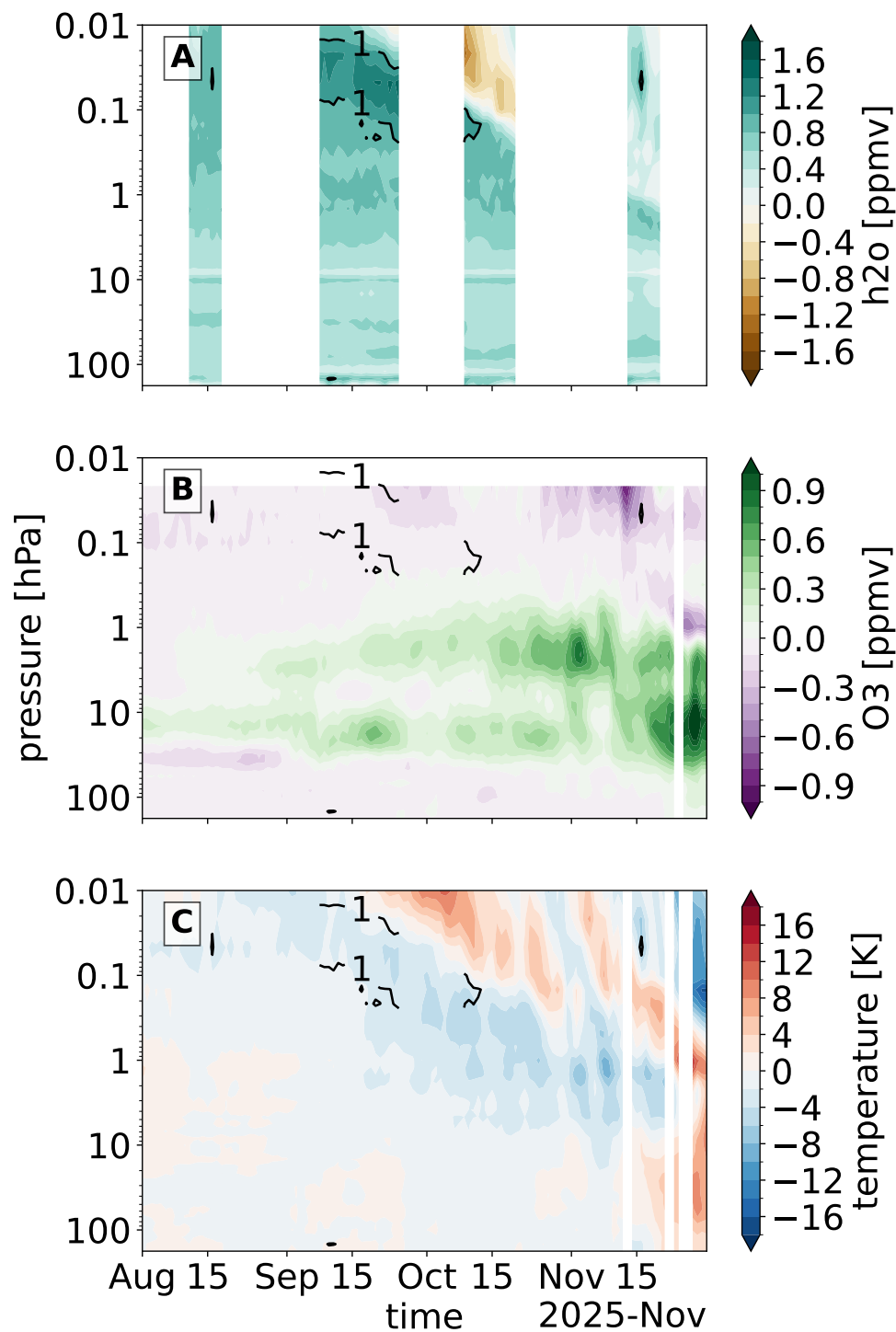


**Figure A3.** As Fig. 2 but for the extended winter 2025/2026.



Since May 2024, the 190 GHz subsystem in MLS, which is responsible for observing water vapor N<sub>2</sub>O, HCN, and upper stratospheric HNO<sub>3</sub>, has been operating on a duty cycle to extend the instrument's lifetime (see <https://mls.jpl.nasa.gov/>). The measurements are reactivated for about six days in the middle of each calendar month. Other MLS channels, including those used for ozone and temperature, remain unaffected.

Temperature and ozone data are processed using the recommended MLS quality screening (QS) criteria, while an adjusted QS is used for the water vapor data. The adjusted QS prevents misclassification of extreme water vapor mixing ratios following the HT eruption (Xu et al., 2022). Due to a retrieval artifact in the 10–8 hPa layer (see Niemeier et al. (2023) and Millán et al. (2024)), we smooth the data vertically.

### 180 A1.3 SWOOSH

The Stratospheric Water and Ozone Satellite Homogenized (SWOOSH) dataset provides zonally averaged monthly profiles for water vapor and ozone. SWOOSH combines measurements from several satellite sensors, including the Stratospheric Aerosol and Gas Experiment (SAGE II & III), the Upper Atmosphere Research Satellite Halogen Occultation Experiment (UARS HALOE), UARS MLS, and Aura MLS. To account for measurement offsets and biases, the data records were homogenized using „reference“ satellites during times in which observations of different satellite systems overlapped. The satellite that showed the best agreement with balloon-based measurements was chosen as a reference (Davis et al., 2016).

## A2 SOCOLv4 simulations

Our set of SOCOLv4 (Sukhodolov et al., 2021) simulations comprises an ensemble of transient simulations with and without the HT forcing, with 5-year spin-up before the HT eruption. Both ensembles comprise 10 ensemble members. We stress that QBO is nudged in both simulations with and without the HT forcing (see Fig. A6). We report the Holton-Tan mechanism (Holton and Tan, 1980) according to equatorial ZW at 10 hPa. For a detailed description of our SOCOLv4 simulations, we refer to Section A1 in Kuchar et al. (2025).

As indicated in Kuchar et al. (2025), the anomalous WV following HT dissipates in SOCOLv4 more quickly, as seen in the observations (cf. globally averaged WV anomaly in SOCOLv4 and SWOOSH in Fig. A1) or the other models (Randel et al., 2024b). Note that the contour for 0.5 ppmv does not reach the year 2024 in SOCOLv4 as in SWOOSH. It is questionable whether this bias is due to a different initialization (Zhu et al., 2025) or a model bias related to the overly fast transport already reported in Sukhodolov et al. (2021); Arsenovic et al. (2019). This longstanding issue persists even in the newest generation of chemistry-climate models, and SOCOLv4 is consistent with other models across generations (Abalos et al., 2026).

## A3 Offline radiative transfer simulations

We prescribed WV and ozone anomalies for 2024-10-10 from MLS and calculated longwave and shortwave radiative heating rates using the 1D radiative convective equilibrium (RCE) model, *konrad* (Kluft et al., 2019; Dacie et al., 2019). See all outputs in Fig. A4. *Konrad* uses the Rapid Radiative Transfer (RT) Model for GCMs and a simple convective adjustment

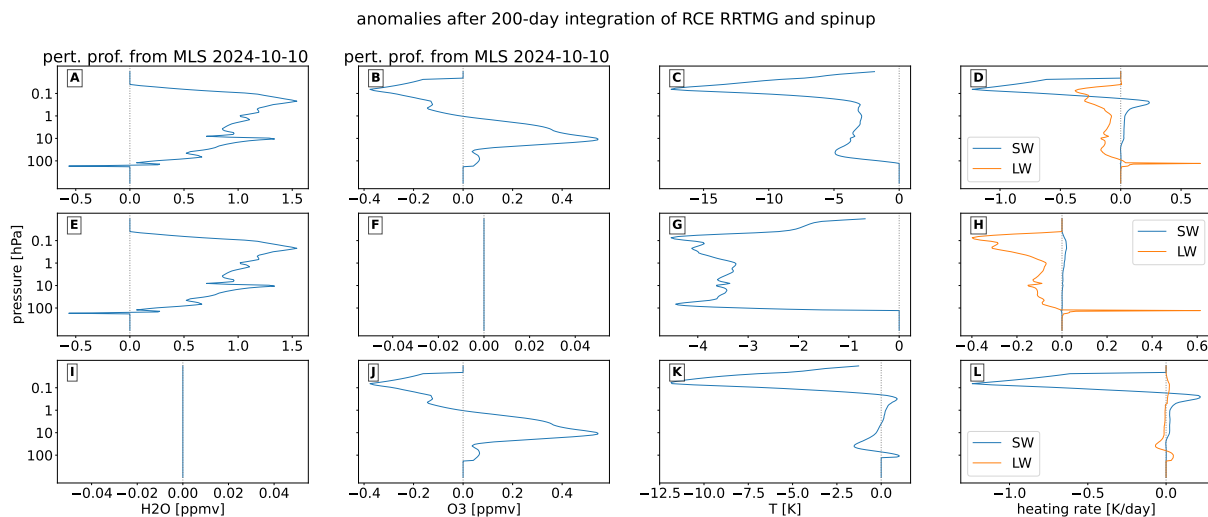


**Figure A4.** Konrad radiative calculations for prescribed water vapour and ozone anomalies from MLS for 2024-10-10.

that fixes tropospheric temperatures up to the convective top according to a moist adiabat, whereas the temperatures in the higher atmospheric levels are determined by radiative–dynamical equilibrium (Kroll et al., 2021). We state that these radiative  
 205 calculations are robust for various solar zenith angles.

The RT calculations are fed with observed WV and O<sub>3</sub> anomaly profiles from MLS. Doing so, we yield negative anomalies in longwave heating rates (of less than  $-0.5\text{ K/day}$ ) throughout the atmospheric layers. These anomalies correspond to the prescribed positive WV anomalies. The RT calculations also yield negative anomalies for shortwave heating rates (exceeding  $-1\text{ K/day}$ ) in the lower mesosphere. These anomalies emerge in consequence of the prescribed negative ozone anomalies.

210 We confirm these calculations using precise line-by-line RT simulations (Bell et al., 2025). The resulting longwave heating rates from prescribed time-evolving WV and ozone from SOCOLv4 are shown in Fig. A5.

As detailed in Bloxam and Huang (2021), the radiative-cooling recovery of SSW-induced temperature anomalies in the absence of dynamical heating is dominated by longwave radiative cooling, and is characterized by increasing  $e$ -folding times from the upper to middle stratosphere. If we invert the  $e$ -folding times ( $4 - 7.5$  days in the upper stratosphere) of Bloxam and  
 215 Huang (2021), we obtain an equivalent heating-rate effect of roughly  $0.13 - -0.25\text{ K} \cdot \text{day}^{-1}$  per K. Given that the  $e$ -folding time increases in the lower stratosphere and decreases in the mesosphere, we expect that temperature perturbations translate into weaker and stronger heating-rate effects at lower and upper levels, respectively. In the lower stratosphere, the air cools more slowly because there is a deeper layer of atmosphere above it that absorbs the radiation, re-emits it upwards but also downwards, and thereby effectively reduces the amount of energy that can escape into space. Closer to the tropopause, the  
 220 cooling effect reduces as the radiation emitted depends strongly on the background temperature itself (Bloxam and Huang, 2021). This asymmetry may explain the differing persistence in the heating rate anomalies at different heights Fig. A5B. Furthermore, the pronounced positive heating rate anomaly around 1 hPa spanning from December 2024 to March 2025,

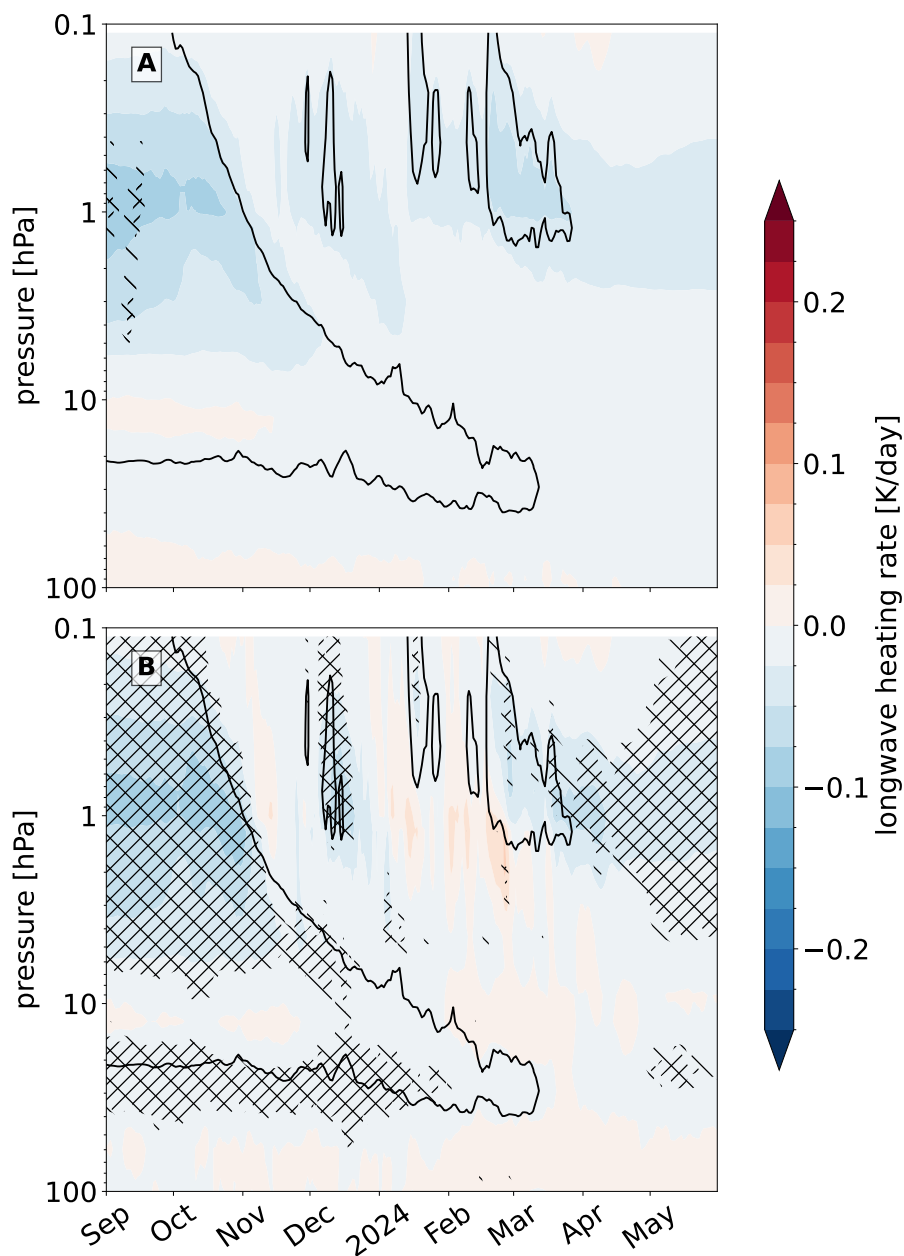


**Figure A5.** Weighted zonally-average over  $60^{\circ}$ – $90^{\circ}$ N of clear-sky (offline) longwave heating rate (in  $\text{K day}^{-1}$ ) anomalies calculated using solely WV (shading in **A**); WV and  $\text{O}_3$  (shading in **B**). Contour in all panels represents a WV anomaly (0.5 ppmv) as in Figure 3. Anomalies are expressed as the difference between the SOCOLv4 simulation with and without the HT forcing. Hatching \\\\\\\\\\\\\ and \\\\\\\\\\\\\\\\\\\\\\\\\\\\\ shows where the p-values of the t-test are  $< 0.1$  and  $< 0.05$ , respectively.



consistent with enhanced short wave absorption related to increased ozone, aids explaining the rapid change from negative to positive temperature anomalies (see Fig. 2B and Fig. 3C).

#### 225 **A4 Calculation of anomalies**

Throughout our analysis, we evaluate significance fields using the minimum local p-values from Student's t-test with global test statistics. All illustrations in Section 2 show differences between simulations with and without the HT forcing.

#### **A5 Eliassen-Palm flux diagnostics**

The response of resolved waves is investigated using the Eliassen-Palm flux diagnostics (EPF; Andrews and McIntyre, 1987). EP fluxes are computed and scaled following Jucker (2021). The EPF convergence serves as an indicator of wave dissipation, and the EPF divergence (EPFD) indicates sourcing. We illustrate all EPF diagnostics from 2023-10-01 to 2024-03-30 in supplementary figure EPFD\_plot\_2023-2024.pdf.

#### **A6 Calculation of Southern Oscillation Index (SOI)**

We calculate the Southern Oscillation Index (SOI) using sea level pressure as a proxy for the El Niño Southern Oscillation. See particular years and corresponding SOI values in Fig. A6.

#### **A7 QBO and ENSO preconditioning**

The episode with the weakened ZW as a consequence of anomalously high EHF in December 2024 (MW3 in Fig. 4) and the beginning of January 2025 can be traced back to two main clusters of ensemble members in the simulations with the HT forcing (see Fig. A7). While one major cluster of 4 ensemble members (with mixed Southern Oscillation Index (SOI) preconditioning) strengthens SPV, the other cluster of 6 ensemble members (with mostly positive SOI (see Appendix A6 and Fig. A6) corresponding to La Niña preconditioning) weakens the stratospheric winds leading to the emergence of SSWs between December 2024 and January 2025. Considering the easterly phase of the Quasi-Biennial Oscillation (QBO) at 10 hPa for MW3, we hypothesize that this may have preconditioned the latter cluster to a higher probability of weaker SPV or SSWs, respectively. Such interpretation is consistent with the observation that SSWs are more likely to occur during easterly QBO in tandem with either El Niño or La Niña conditions (Lee et al., 2025).

That said, the simulated equatorial winds in the westerly QBO phase during the early stage of MW2 (see Fig. A6) create conditions that favor a stronger SPV, consistent with the Holton–Tan mechanism (Holton and Tan, 1980). A similar configuration occurred in OW3, when the QBO was also in its westerly phase<sup>1</sup>. Since the QBO preconditioning is identical in both simulations (with and without the HT forcing) and ENSO is uniformly sampled in SOCOLv4, encompassing both El Niño (SOI<0) and La Niña (SOI>0; as ultimately observed in OW3), we infer that the forced SPV response in MW2 arises from the HT-induced WV.

<sup>1</sup><https://www.climate.gov/news-features/blogs/polar-vortex/predicting-chances-polar-vortex-disruption-winter>

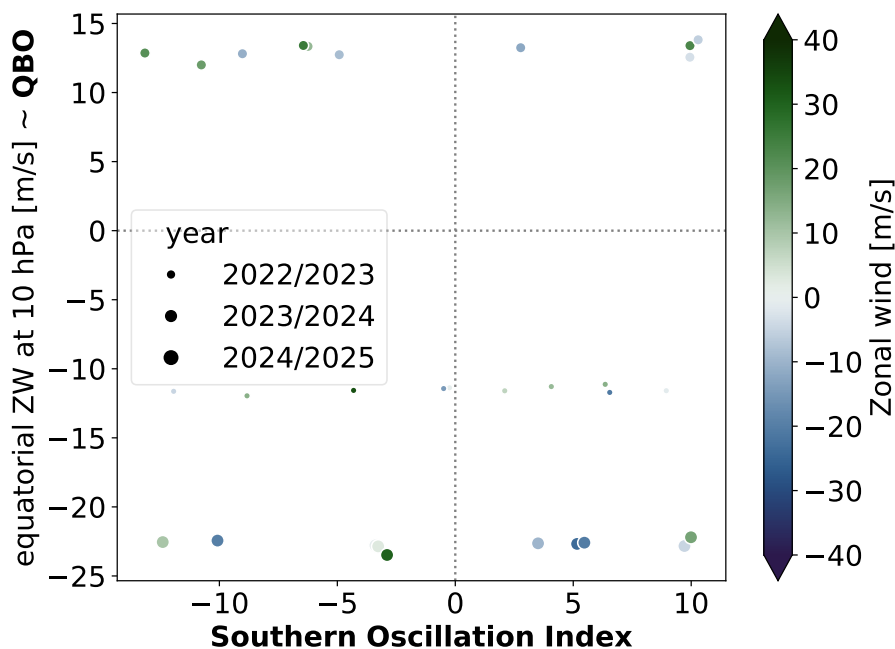


**Figure A6.** Scatter plot of equatorial zonal wind at 10hPa as a proxy for Quasi-biennial Oscillation (QBO) in SOCOLv4 and Southern Oscillation Index (SOI) in the simulation with the HT forcing. Individual years and their corresponding zonal wind anomalies at 60°N as in Figs. 3 and 4.

From the SOCOLv4 ensemble, yielding one cluster with easterly QBO and La Nina conditions in MW3, we hypothesize that the winter 2025/2026 (OW4) bears an enhanced probability of SSW occurrence. As the associated wind pattern propagates downward, we consequently identify a sea level pressure (SLP) pattern characteristic of a weaker SPV, i.e., a positive SLP anomaly at the poles and a negative SLP anomaly at the mid-latitudes (see Fig. A8).

255

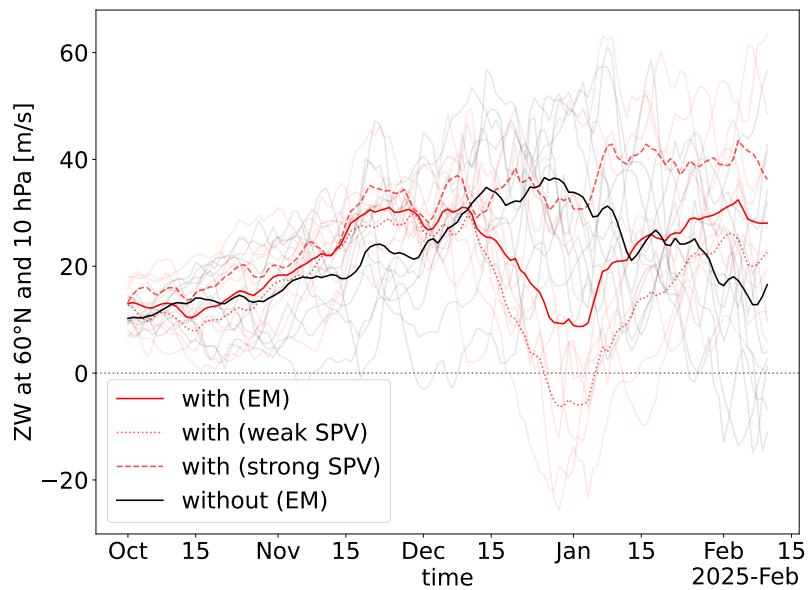


**Figure A7.** Daily zonal-mean zonal wind at 10 hPa and 60°N based on the SOCOLv4 simulation with (ensemble mean (EM); red solid line) and without (black solid line) the HT forcing for the period 2024/2025 (MW3). The SOCOLv4 simulation with the HT forcing reveals two clusters: weak SPV (red dotted line) and strong SPV (red dashed line).



## February 2025

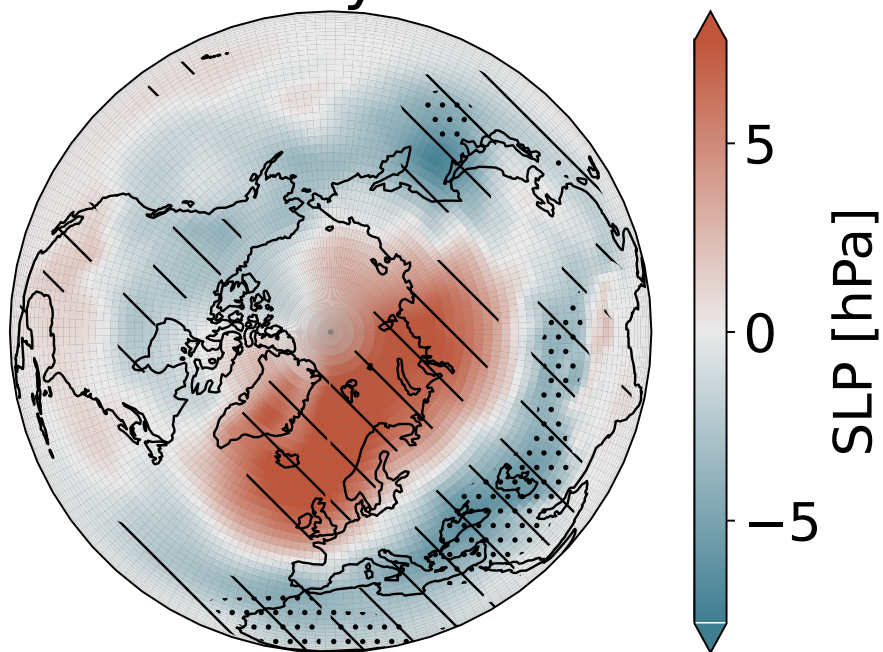


**Figure A8.** Monthly anomaly of Sea level pressure (SLP in hPa) in February 2025 (MW3). Anomalies are expressed as the difference between the SOCOLv4 simulation with and without the HT forcing.  $2\sigma$  statistical significance from the t-test is indicated by dots.  $1\sigma$  statistical significance from the t-test is indicated by hatching.



*Author contributions.* AK designed the study. TS set up and carried out the model simulations. AK analysed the data. AK, BL, JKH, TS, MS, and AB curated the data. AK compiled the manuscript with inputs from all other authors.

*Competing interests.* The authors declare that they have no conflict of interest.

*Acknowledgements.* ER has been supported by St. Petersburg State University under research grant 124032000025-1. MS was funded by the  
260 University of Graz, Graz, Austria. AB has been supported by the "Swiss H<sub>2</sub>O Hub for High-quality water vapor measurements from ground to space" project financed by GAW Switzerland.



## References

- Abalos, M., Birner, T., Chrysanthou, A., Davis, S., de la Cámara, A., Dhomse, S., Garny, H., Hegglin, M. I., Hubert, D., Ivaniha, O., Keeble, J., Linz, M., Minganti, D., Neu, J., Plummer, D., Saunders, L., Shah, K., Stiller, G., Tourpali, K., Waugh, D., Abraham, N. L., Akiyoshi, H., Chipperfield, M. P., Jöckel, P., Josse, B., Morgenstern, O., Sukhodolov, T., Watanabe, S., and Yamashita, Y.: Evaluation of stratospheric transport in three generations of Chemistry-Climate Models, *EGUsphere*, 2026, 1–61, <https://doi.org/10.5194/egusphere-2025-6549>, 2026.
- Andrews, D. G. and McIntyre, M. E.: JR Holton, and CB Leovy, 1987: *Middle Atmosphere Dynamics*, 1987.
- APARC: The Hunga Volcanic Eruption Atmospheric Impacts Report, APARC Report 11, World Climate Research Programme (WCRP), <https://doi.org/10.34734/FZJ-2025-05237>, wCRP Report 10/2025, 2025.
- 265 Arsenovic, P., Damiani, A., Rozanov, E., Funke, B., Stenke, A., and Peter, T.: Reactive nitrogen ( $\text{NO}_y$ ) and ozone responses to energetic electron precipitation during Southern Hemisphere winter, *Atmospheric Chemistry and Physics*, 19, 9485–9494, <https://doi.org/10.5194/acp-19-9485-2019>, 2019.
- Bednarz, E. M., Butler, A. H., Wang, X., Zhuo, Z., Yu, W., Stenchikov, G., Toohey, M., and Zhu, Y.: Indirect climate impacts of the Hunga eruption, *Atmospheric Chemistry and Physics*, 26, 197–215, <https://doi.org/10.5194/acp-26-197-2026>, 2026.
- 275 Bell, A., Murk, A., and Stober, G.: Radiative impact of increased middle atmospheric water vapour in the aftermath of the Hunga 2022 volcanic eruption at two locations in the Northern Hemisphere, *EGUsphere*, 2025, 1–22, <https://doi.org/10.5194/egusphere-2025-1396>, 2025.
- Bittner, M., Schmidt, H., Timmreck, C., and Sienz, F.: Using a large ensemble of simulations to assess the Northern Hemisphere stratospheric dynamical response to tropical volcanic eruptions and its uncertainty, *Geophysical Research Letters*, 43, 9324–9332, <https://doi.org/https://doi.org/10.1002/2016GL070587>, 2016a.
- 280 Bittner, M., Timmreck, C., Schmidt, H., Toohey, M., and Krüger, K.: The impact of wave-mean flow interaction on the Northern Hemisphere polar vortex after tropical volcanic eruptions, *Journal of Geophysical Research: Atmospheres*, 121, 5281–5297, <https://doi.org/https://doi.org/10.1002/2015JD024603>, 2016b.
- Bloxam, K. and Huang, Y.: Radiative Relaxation Time Scales Quantified from Sudden Stratospheric Warmings, *Journal of the Atmospheric Sciences*, 78, 269 – 286, <https://doi.org/10.1175/JAS-D-20-0015.1>, 2021.
- 285 Brasseur, G. P. and Solomon, S.: *Aeronomy of the middle atmosphere: Chemistry and physics of the stratosphere and mesosphere*, vol. 32, Springer Science & Business Media, 2005.
- Charney, J. G. and Drazin, P. G.: Propagation of planetary-scale disturbances from the lower into the upper atmosphere, *Journal of Geophysical Research*, 66, 83–109, 1961.
- 290 Clough, S. A. and Iacono, M. J.: Line-by-line calculation of atmospheric fluxes and cooling rates: 2. Application to carbon dioxide, ozone, methane, nitrous oxide and the halocarbons, *Journal of Geophysical Research: Atmospheres*, 100, 16 519–16 535, 1995.
- Dacie, S., Kluft, L., Schmidt, H., Stevens, B., Buehler, S. A., Nowack, P. J., Dietmüller, S., Abraham, N. L., and Birner, T.: A 1D RCE Study of Factors Affecting the Tropical Tropopause Layer and Surface Climate, *Journal of Climate*, 32, 6769 – 6782, <https://doi.org/10.1175/JCLI-D-18-0778.1>, 2019.
- 295 Davis, S. M., Rosenlof, K. H., Hassler, B., Hurst, D. F., Read, W. G., Vömel, H., Selkirk, H., Fujiwara, M., and Damadeo, R.: The Stratospheric Water and Ozone Satellite Homogenized (SWOOSH) database: a long-term database for climate studies, *Earth System Science Data*, 8, 461–490, <https://doi.org/10.5194/essd-8-461-2016>, 2016.



- 300 Evan, S., Brioude, J., Rosenlof, K. H., Gao, R.-S., Portmann, R. W., Zhu, Y., Volkamer, R., Lee, C. F., Metzger, J.-M., Lamy, K., Walter, P., Alvarez, S. L., Flynn, J. H., Asher, E., Todt, M., Davis, S. M., Thornberry, T., Vömel, H., Wienhold, F. G., Stauffer, R. M., Millán, L., Santee, M. L., Froidevaux, L., and Read, W. G.: Rapid ozone depletion after humidification of the stratosphere by the Hunga Tonga Eruption, *Science*, 382, eadg2551, <https://doi.org/10.1126/science.adg2551>, 2023.
- Fleming, E. L., Newman, P. A., Liang, Q., and Oman, L. D.: Stratospheric Temperature and Ozone Impacts of the Hunga Tonga-Hunga Ha'apai Water Vapor Injection, *Journal of Geophysical Research: Atmospheres*, 129, e2023JD039298, <https://doi.org/https://doi.org/10.1029/2023JD039298>, e2023JD039298 2023JD039298, 2024.
- 305 Funke, B., López-Puertas, M., Stiller, G. P., and von Clarmann, T.: Mesospheric and stratospheric NO<sub>y</sub> produced by energetic particle precipitation during 2002–2012, *Journal of Geophysical Research: Atmospheres*, 119, 4429–4446, <https://doi.org/https://doi.org/10.1002/2013JD021404>, 2014.
- Gelaro, R., McCarty, W., Suárez, M. J., Todling, R., Molod, A., Takacs, L., Randles, C. A., Darmenov, A., Bosilovich, M. G., Reichle, R., Wargan, K., Coy, L., Cullather, R., Draper, C., Akella, S., Buchard, V., Conaty, A., da Silva, A. M., Gu, W., Kim, G.-K., Koster, R., 310 Lucchesi, R., Merkova, D., Nielsen, J. E., Partyka, G., Pawson, S., Putman, W., Rienecker, M., Schubert, S. D., Sienkiewicz, M., and Zhao, B.: The Modern-Era Retrospective Analysis for Research and Applications, Version 2 (MERRA-2), *Journal of Climate*, 30, 5419 – 5454, <https://doi.org/10.1175/JCLI-D-16-0758.1>, 2017.
- Holton, J. R. and Tan, H.-C.: The influence of the equatorial quasi-biennial oscillation on the global circulation at 50 mb, *Journal of Atmospheric Sciences*, 37, 2200–2208, 1980.
- 315 Jenkins, S., Smith, C., Allen, M., and Grainger, R.: Tonga eruption increases chance of temporary surface temperature anomaly above 1.5° C, *Nature Climate Change*, 13, 127–129, 2023.
- Joshi, M. M., Charlton, A. J., and Scaife, A. A.: On the influence of stratospheric water vapor changes on the tropospheric circulation, *Geophysical Research Letters*, 33, <https://doi.org/https://doi.org/10.1029/2006GL025983>, 2006.
- Jucker, M.: Scaling of Eliassen-Palm flux vectors, *Atmospheric Science Letters*, 22, e1020, <https://doi.org/https://doi.org/10.1002/asl.1020>, 320 2021.
- Keeble, J., Braesicke, P., Abraham, N. L., Roscoe, H. K., and Pyle, J. A.: The impact of polar stratospheric ozone loss on Southern Hemisphere stratospheric circulation and climate, *Atmospheric Chemistry and Physics*, 14, 13 705–13 717, <https://doi.org/10.5194/acp-14-13705-2014>, publisher: Copernicus GmbH, 2014.
- Kluft, L., Dacie, S., Buehler, S. A., Schmidt, H., and Stevens, B.: Re-Examining the First Climate Models: Climate Sensitivity of a Modern 325 Radiative–Convective Equilibrium Model, *Journal of Climate*, 32, 8111 – 8125, <https://doi.org/10.1175/JCLI-D-18-0774.1>, 2019.
- Kramarova, N. and Lait, L. R.: NASA Ozone Watch: 2025 Antarctic MERRA-2 Wind, [https://ozonewatch.gsfc.nasa.gov/meteorology/ozone\\_2024\\_MERRA2\\_NH.html](https://ozonewatch.gsfc.nasa.gov/meteorology/ozone_2024_MERRA2_NH.html), last updated 2025-12-19 21:55:40Z, 2025.
- Kroll, C. A. and Schmidt, A.: Indirect stratospheric moisture increase after a Pinatubo-magnitude eruption can be comparable to direct increase after 2022 Hunga, *Communications Earth & Environment*, 5, 497, 2024.
- 330 Kroll, C. A., Dacie, S., Azoulay, A., Schmidt, H., and Timmreck, C.: The impact of volcanic eruptions of different magnitude on stratospheric water vapor in the tropics, *Atmospheric Chemistry and Physics*, 21, 6565–6591, <https://doi.org/10.5194/acp-21-6565-2021>, 2021.
- Kuchar, A., Sukhodolov, T., Chiodo, G., Jörmann, A., Kult-Herdin, J., Rozanov, E., and Rieder, H. H.: Modulation of the northern polar vortex by the Hunga Tonga–Hunga Ha'apai eruption and the associated surface response, *Atmospheric Chemistry and Physics*, 25, 3623–3634, <https://doi.org/10.5194/acp-25-3623-2025>, 2025.



- 335 Lawrence, Z. D., Perlwitz, J., Butler, A. H., Manney, G. L., Newman, P. A., Lee, S. H., and Nash, E. R.: The Remarkably Strong Arctic Stratospheric Polar Vortex of Winter 2020: Links to Record-Breaking Arctic Oscillation and Ozone Loss, *Journal of Geophysical Research: Atmospheres*, 125, e2020JD033271, <https://doi.org/https://doi.org/10.1029/2020JD033271>, e2020JD033271 10.1029/2020JD033271, 2020.
- Lee, S. H., Butler, A. H., and Manney, G. L.: Two major sudden stratospheric warmings during winter 2023/2024, *Weather*, 80, 45–53, <https://doi.org/https://doi.org/10.1002/wea.7656>, 2025.
- 340 Livesey, N., Read, W., Wagner, P., Froidevaux, L., Santee, M., Schwartz, M., Lambert, A., Millan Valle, L., Pumphrey, H., Manney, G., et al.: Earth observing system (EOS) aura microwave limb sounder (MLS) version 5.0 x level 2 and 3 data quality and description document, JPL D-105336 Rev, 2022.
- Manney, G. L., Santee, M. L., Rex, M., Livesey, N. J., Pitts, M. C., Veefkind, P., Nash, E. R., Wohltmann, I., Lehmann, R., Froidevaux, L., et al.: Unprecedented Arctic ozone loss in 2011, *Nature*, 478, 469–475, <https://doi.org/https://doi.org/10.1038/nature10556>, 2011.
- 345 Manzini, E., Steil, B., Brühl, C., Giorgetta, M. A., and Krüger, K.: A new interactive chemistry-climate model: 2. Sensitivity of the middle atmosphere to ozone depletion and increase in greenhouse gases and implications for recent stratospheric cooling, *Journal of Geophysical Research: Atmospheres*, 108, <https://doi.org/https://doi.org/10.1029/2002JD002977>, [\\_eprint: https://agupubs.onlinelibrary.wiley.com/doi/pdf/10.1029/2002JD002977](https://agupubs.onlinelibrary.wiley.com/doi/pdf/10.1029/2002JD002977), 2003.
- Matthias, V., Dörnbrack, A., and Stober, G.: The extraordinarily strong and cold polar vortex in the early northern winter 2015/2016, *Geophysical Research Letters*, 43, 12,287–12,294, <https://doi.org/https://doi.org/10.1002/2016GL071676>, 2016.
- 350 Maycock, A. C., Joshi, M. M., Shine, K. P., and Scaife, A. A.: The Circulation Response to Idealized Changes in Stratospheric Water Vapor, *Journal of Climate*, 26, 545 – 561, <https://doi.org/10.1175/JCLI-D-12-00155.1>, 2013.
- Millán, L., Santee, M. L., Lambert, A., Livesey, N. J., Werner, F., Schwartz, M. J., Pumphrey, H. C., Manney, G. L., Wang, Y., Su, H., Wu, L., Read, W. G., and Froidevaux, L.: The Hunga Tonga-Hunga Ha’apai Hydration of the Stratosphere, *Geophysical Research Letters*, 49, e2022GL099381, <https://doi.org/https://doi.org/10.1029/2022GL099381>, e2022GL099381 2022GL099381, 2022.
- 355 Millán, L., Read, W. G., Santee, M. L., Lambert, A., Manney, G. L., Neu, J. L., Pitts, M. C., Werner, F., Livesey, N. J., and Schwartz, M. J.: The Evolution of the Hunga Hydration in a Moistening Stratosphere, *Geophysical Research Letters*, 51, e2024GL110841, <https://doi.org/https://doi.org/10.1029/2024GL110841>, e2024GL110841 2024GL110841, 2024.
- Newman, P. A., Nash, E. R., and Rosenfield, J. E.: What controls the temperature of the Arctic stratosphere during the spring?, *Journal of Geophysical Research: Atmospheres*, 106, 19999–20010, <https://doi.org/https://doi.org/10.1029/2000JD000061>, 2001.
- 360 Niemeier, U., Wallis, S., Timmreck, C., van Pham, T., and von Savigny, C.: How the Hunga Tonga—Hunga Ha’apai Water Vapor Cloud Impacts Its Transport Through the Stratosphere: Dynamical and Radiative Effects, *Geophysical Research Letters*, 50, e2023GL106482, <https://doi.org/https://doi.org/10.1029/2023GL106482>, e2023GL106482 2023GL106482, 2023.
- Plumb, R. A.: On the seasonal cycle of stratospheric planetary waves, *Pure and applied geophysics*, 130, 233–242, 1989.
- 365 Proud, S. R., Prata, A. T., and Schmauß, S.: The January 2022 eruption of Hunga Tonga-Hunga Ha’apai volcano reached the mesosphere, *Science*, 378, 554–557, <https://doi.org/10.1126/science.abo4076>, 2022.
- Randel, W. J., Podglajen, A., and Wu, F.: Stratospheric Transit Time Distributions Derived From Satellite Water Vapor Measurements, *Journal of Geophysical Research: Atmospheres*, 129, e2024JD041595, <https://doi.org/https://doi.org/10.1029/2024JD041595>, e2024JD041595 2024JD041595, 2024a.
- 370 Randel, W. J., Wang, X., Starr, J., Garcia, R. R., and Kinnison, D.: Long-Term Temperature Impacts of the Hunga Volcanic Eruption in the Stratosphere and Above, *Geophysical Research Letters*, 51, e2024GL111500, <https://doi.org/https://doi.org/10.1029/2024GL111500>, [\\_eprint: https://onlinelibrary.wiley.com/doi/pdf/10.1029/2024GL111500](https://onlinelibrary.wiley.com/doi/pdf/10.1029/2024GL111500), 2024b.



- Rieder, H., Kult-Herdin, J., Polvani, L. M., Solomon, S., and Kuchar, A.: Are springtime Arctic ozone columns predictable from wintertime conditions?, *Frontiers in Earth Science*, 13, 1610651, <https://doi.org/https://doi.org/10.3389/feart.2025.1610651>, 2025.
- 375 Rupp, P., Spaeth, J., and Birner, T.: A spread-versus-error framework to reliably quantify the potential for subseasonal windows of forecast opportunity, *EGUsphere*, 2025, 1–24, <https://doi.org/10.5194/egusphere-2025-4925>, 2025.
- Schoeberl, M. R., Wang, Y., Ueyama, R., Dessler, A., Taha, G., and Yu, W.: The Estimated Climate Impact of the Hunga Tonga-Hunga Ha’apai Eruption Plume, *Geophysical Research Letters*, 50, e2023GL104634, <https://doi.org/10.1029/2023GL104634>, 2023.
- Schoeberl, M. R., Toohey, M., Wang, Y., and Ueyama, R.: Stratospheric Injection Lifetimes, *Journal of Geophysical Research: Atmospheres*, 380 130, e2025JD043928, <https://doi.org/https://doi.org/10.1029/2025JD043928>, e2025JD043928 2025JD043928, 2025.
- Scott, R. and Haynes, P.: The seasonal cycle of planetary waves in the winter stratosphere, *Journal of the atmospheric sciences*, 59, 803–822, 2002.
- Seabrook, M., Smith, D. M., Dunstone, N. J., Eade, R., Hermanson, L., Scaife, A. A., and Hardiman, S. C.: Opposite Impacts of Interannual and Decadal Pacific Variability in the Extratropics, *Geophysical Research Letters*, 50, e2022GL101226, 385 <https://doi.org/https://doi.org/10.1029/2022GL101226>, e2022GL101226 2022GL101226, 2023.
- Seppälä, A., Kalakoski, N., Verronen, P. T., Marsh, D. R., Karpechko, A. Y., and Szélag, M. E.: Polar mesospheric ozone loss initiates downward coupling of solar signal in the Northern Hemisphere, *Nature Communications*, 16, 748, 2025.
- Stenchikov, G., Ukhov, A., and Osipov, S.: Modeling the Radiative Forcing and Atmospheric Temperature Perturbations Caused by the 2022 Hunga Volcano Explosion, *Journal of Geophysical Research: Atmospheres*, 130, e2024JD041940, 390 <https://doi.org/10.1029/2024JD041940>, 2025.
- Stocker, M., Steiner, A. K., Ladstädter, F., Foelsche, U., and Randel, W. J.: Strong persistent cooling of the stratosphere after the Hunga eruption, *Communications Earth & Environment*, 5, 450, <https://doi.org/https://doi.org/10.1038/s43247-024-01620-3>, 2024.
- Sukhodolov, T., Egorova, T., Stenke, A., Ball, W. T., Brodowsky, C., Chiodo, G., Feinberg, A., Friedel, M., Karagodin-Doyennel, A., Peter, T., Sedlacek, J., Vattioni, S., and Rozanov, E.: Atmosphere–ocean–aerosol–chemistry–climate model SOCOLv4.0: description and 395 evaluation, *Geoscientific Model Development*, 14, 5525–5560, <https://doi.org/10.5194/gmd-14-5525-2021>, 2021.
- Vömel, H., Evan, S., and Tully, M.: Water vapor injection into the stratosphere by Hunga Tonga-Hunga Ha’apai, *Science*, 377, 1444–1447, <https://doi.org/10.1126/science.abq2299>, 2022.
- Waters, J. W., Froidevaux, L., Harwood, R. S., Jarnot, R. F., Pickett, H. M., Read, W. G., Siegel, P. H., Cofield, R. E., Filipiak, M. J., Flower, D. A., et al.: The earth observing system microwave limb sounder (EOS MLS) on the Aura satellite, *IEEE transactions on geoscience and 400 remote sensing*, 44, 1075–1092, 2006.
- Xu, J., Li, D., Bai, Z., Tao, M., and Bian, J.: Large amounts of water vapor were injected into the stratosphere by the Hunga Tonga–Hunga Ha’apai volcano eruption, *Atmosphere*, 13, 912, 2022.
- Young, P. J., Butler, A. H., Calvo, N., Haimberger, L., Kushner, P. J., Marsh, D. R., Randel, W. J., and Rosenlof, K. H.: Agreement in late twentieth century Southern Hemisphere stratospheric temperature trends in observations and CCMVal-2, CMIP3, and CMIP5 models, 405 *Journal of Geophysical Research: Atmospheres*, 118, 605–613, <https://doi.org/10.1002/jgrd.50126>, publisher: John Wiley & Sons, Ltd, 2013.
- Zhou, X., Dhomse, S. S., Feng, W., Mann, G., Heddell, S., Pumphrey, H., Kerridge, B. J., Latter, B., Siddans, R., Ventress, L., Querel, R., Smale, P., Asher, E., Hall, E. G., Bekki, S., and Chipperfield, M. P.: Antarctic Vortex Dehydration in 2023 as a Substantial Removal Pathway for Hunga Tonga-Hunga Ha’apai Water Vapor, *Geophysical Research Letters*, 51, e2023GL107630, 410 <https://doi.org/https://doi.org/10.1029/2023GL107630>, e2023GL107630 2023GL107630, 2024.



Zhu, Y., Akiyoshi, H., Aquila, V., Asher, E., Bednarz, E. M., Bekki, S., Brühl, C., Butler, A. H., Case, P., Chabrillat, S., Chiodo, G., Clyne, M., Colarco, P. R., Dhomse, S., Falletti, L., Fleming, E., Johnson, B., Jörimann, A., Kovilakam, M., Koren, G., Kuchar, A., Lebas, N., Liang, Q., Liu, C.-C., Mann, G., Manyin, M., Marchand, M., Morgenstern, O., Newman, P., Oman, L. D., Østerstrøm, F. F., Peng, Y., Plummer, D., Quaglia, I., Randel, W., Rémy, S., Sekiya, T., Steenrod, S., Sukhodolov, T., Tilmes, S., Tsigaridis, K., Ueyama, R., Visioni, D., Wang, X., Watanabe, S., Yamashita, Y., Yu, P., Yu, W., Zhang, J., and Zhuo, Z.: Hunga Tonga–Hunga Ha'apai Volcano Impact Model Observation Comparison (HTHH-MOC) project: experiment protocol and model descriptions, *Geoscientific Model Development*, 18, 5487–5512, <https://doi.org/10.5194/gmd-18-5487-2025>, 2025.

Zhuo, Z., Wang, X., Zhu, Y., Yu, W., Bednarz, E. M., Fleming, E., Colarco, P. R., Watanabe, S., Plummer, D., Stenchikov, G., Randel, W., Bourassa, A., Aquila, V., Sekiya, T., Schoeberl, M. R., Tilmes, S., Zhang, J., Kushner, P. J., and Pausata, F. S. R.: Comparing multi-model ensemble simulations with observations and decadal projections of upper atmospheric variations following the Hunga eruption, *Atmospheric Chemistry and Physics*, 25, 13 161–13 176, <https://doi.org/10.5194/acp-25-13161-2025>, 2025.